energies

MDPI

Article

Experimental Investigation of a 10 MW Prototype Kaplan Turbine during Start-Up Operation

Arash Soltani Dehkharqani [1,*], Fredrik Engström [1], Jan-Olov Aidanpää [2] and Michel J. Cervantes [1]

[1] Division of Fluid and Experimental Mechanics, Luleå University of Technology, SE-971 87 Luleå, Sweden; fredrik.1.engstrom@ltu.se (F.E.); michel.cervantes@ltu.se (M.J.C.)
[2] Division of Product and Production Development, Luleå University of Technology, SE-971 87 Luleå, Sweden; jan-olov.aidanpaa@ltu.se
* Correspondence: arasol@ltu.se; Tel.: +46-920-493404

Received: 18 October 2019; Accepted: 27 November 2019; Published: 2 December 2019

Abstract: An increase in the start/stop cycles of hydraulic turbines due to the penetration of intermittent renewable energy sources is important. Hydraulic instabilities that occur in hydraulic turbines during start/stops may cause structural issues in the turbine components. High-stress fluctuations on the runner blades are expected during start-ups due to the unsteady pressure loading on the runner blades. This paper presents experiments performed on a 10 MW prototype Kaplan turbine at the Porjus Hydropower Center during a start-up cycle. Synchronized unsteady pressure and strain measurements on a runner blade and axial, bending (in two directions) and torsion strain measurements on the shaft were performed. In addition, the general parameters of the turbine (e.g., rotational speed, guide vane opening and runner blade angle) were acquired. Low-frequency fluctuations (0–15 Hz) were observed in the pressure data on the runner blade after opening the guide vanes from the completely closed position. A higher strain value was observed on the strain gauges installed on the runner blade near the hub (200–500 μm/m) compared to the ones near the shroud at the leading and trailing edge. The strain fluctuation level on the shaft decreased after loading the generator by further opening the guide vanes. Higher fluctuations were observed in the torsion strain compared to axial and bending strain. In addition, the torsion strain peak-to-peak value reached 12 times its corresponding value at 61% guide vane opening.

Keywords: prototype Kaplan turbine; start-up; pressure measurement; strain measurement; axial strain; bending strain; torsion strain

1. Introduction

Hydraulic turbines are widely used for flexible electricity generation, including frequency control, because the amount of produced electricity from intermittent renewable energy sources has considerably increased. Consequently, these turbines operate under a larger range of discharge values and undergo more transient operations than what they were initially designed for. Transient operations consist of load variation, start, stop, speed-no-load, runaway and emergency shutdown, where the last two operations represent non-normal operation. Severe hydrodynamic conditions may provoke high-pressure fluctuations in the turbine, particularly on the runner blades [1]. This outcome directly affects the unit operational lifetime and imposes more regular refurbishment requirements [2,3].

During the start-up cycle, the runner accelerates from zero to synchronous speed, which is called speed-no-load operation. After the runner speed is stabilized, the generator is magnetized, and the guide vane opening increases to the set value. The unsteady flow leaving the runner has a large swirl during the start-up operation [4]. Low-frequency transient loads that occur on the runner blades induce

slow cycle fatigue [5]. In addition, high amplitude vibrations can occur due to the resonance between the low frequencies developed during the start-up operation and the natural frequencies of the runner. The runner blades experience random and periodic stress that is induced by stochastic and periodic flow during the start-up cycle [5–7]. The damage to the runner blade caused by one start-up cycle to a runner blade was observed to be equivalent to thirty years of turbine operation under a partial load operating condition, approximately 60% of the best efficiency point where the pressure pulsations in the draft tube are maximum [8]. In addition, no clear correlation between pressure pulsations in the draft tube and strain values on the runner blade was observed.

Guide vane opening limit and opening rate are two parameters that can influence pressure fluctuations in the turbine during the start-up operation. A start-up operation creates a complex flow and stochastic pressure loads in the turbine due to the change in the runner speed and transient pressure variation. The startup and shutdown scheme are defined during the turbine commissioning and can be changed during the refurbishment in power plants. An optimized start-up and shutdown scheme can reduce the damage and increase the life expectancy [9]. Nevertheless, this operation should be performed on a case-by-case basis because each turbine exhibits a unique behavior during a start-up cycle, and general methods have not yet been proposed [10]. An optimized start-up sequence was obtained by performing strain measurements on the runner blade of a prototype propeller turbine during the turbine commissioning [10]. Different start-up strategies were investigated. The optimization was based on maximizing the fatigue reliability during the lifetime of the runner. Although the maximum strain in the runner blade did not decrease during the optimized start-up, the strain transient fluctuation decreased at the beginning of the cycle. Another study showed that the reduction in the guide vane opening rate could reduce the crack propagation rate on the runner blades of a prototype Francis turbine [11]. In addition to fatigue issues, different natural frequencies can be excited during the start-up process by the initial hit of the water on the runner blades and later by the rotor-stator interaction [12]. High amplitude pressure fluctuations were observed in the draft tube of two prototype Francis turbines during the guide vane opening from a closed position to the generator synchronization [13]. Moreover, the pressure amplitudes increased during the synchronization process. Axial and torsion strain measurements were performed on the shaft of a prototype Kaplan turbine during a start-up operation [14]. A wide-band frequency (high intensity of approximately 0–5 Hz for a short period of time) was observed before reaching the synchronous speed.

A series of measurements were performed on a Francis turbine model installed at the Water Power Laboratory (WPL), Norwegian University of Science and Technology, Norway. Unsteady pressure measurements on the runner blades, in the vaneless space, and in the draft tube of a high head Francis turbine model were carried out during start-up and shut down cycles in an open-loop test rig [15]. Three start-up and three shut down guide vane opening schemes were examined. The pressure fluctuations in the runner during the rapid start-up scheme were observed to be approximately 1.5 times their corresponding values during the slow opening scheme. Another study on the same facility was performed to investigate the speed-no-load condition [16]. High-pressure fluctuations were obtained compared to the normal operating point, i.e., the best efficiency point. Goyal et al. [4] performed synchronized flow measurements using particle image velocimetry and pressure measurements during the start-up operation. An asymmetric flow concentrating towards the right wall of the draft tube was observed during the initial phase of the start-up. Amiri et al. [17] showed that the asymmetry in the flow after the runner is associated with the Dean vortices that appear after the draft tube elbow. The strength of these vortices can be altered by the swirl leaving the runner. Recently, Coulaud et al. [18] investigated the start-up sequence of a bulb turbine model by considering three different guide vane opening speeds in a closed-loop circuit at the Hydraulic Machine Laboratory, Laval University, Canada. One of the main challenges in a closed-loop model test is to maintain the turbine head using air injection in the upstream reservoir [19]. Unsteady pressure measurements on the runner blade were performed, and the pressure field was estimated using an interpolation technique. It was observed

that the guide vane opening rate was an important parameter that affected the pressure distribution on the runner blade.

It is difficult to simulate the start-up or shutdown of a prototype turbine due to the computational cost attributed to the wide range of time scales that arise from the turbine operational time, which can be as high as 30–40 s, and as low as 0.01 s for the rotor-stator interaction. Moreover, boundary conditions (e.g., transient inlet and outlet of the turbine, guide vane movement, variable rotational speed and variable runner blade) have to be carefully treated in numerical simulations. Nicolle et al. [20] performed numerical flow simulations of a low head Francis turbine during the start-up. Two start-up scenarios were studied. The obtained pressure value on the blade leading edge showed that although the maximum pressure was captured, the pressure fluctuation was damped compared to the experimental data. Later, structural analysis was performed on the same test case [21]. An overall trend of the mean strain was correctly predicted but the strain fluctuations were not obtained. Recently, one-way fluid-structure coupled simulations were performed on a medium head Francis turbine to investigate the stochastic strain on the runner blade [22]. The synchronous speed was overpredicted by approximately 10%. The stochastic loads were only partially captured on the leading edge. It was mentioned that two-way coupling was needed to obtain the correct blade loading at the trailing edge. In addition, cavitation was not included in the analysis. A prototype pump-turbine was numerically investigated during the start-up operation [23]. At the beginning of the start-up, the flow after the guide vanes formed a ring-shaped structure that became very strong at speed-no-load. The results showed that the pressure fluctuations close to the stay vanes and in the draft tube during the speed-no-load could reach 3.8–8 times that at full load. In addition, the fluctuation of radial and tangential forces on the runner increased by reaching the synchronous speed, which implied the non-uniform flow on the runner blades.

Compared with prototype turbines, the numerical simulations of model turbines, including flow simulations and fluid-structure coupled simulations, are affordable during the start-up operation [24–27]. Numerical simulations showed an overestimation of the synchronous speed by 5% for a bulb turbine model during speed-no-load [26]. One-way fluid-structure coupling was used to predict the strain value on the runner blade. The mean strain value was correctly captured while the strain fluctuations were underestimated by a factor of two. A pump-turbine model was numerically investigated during the start-up [27]. Pressure fluctuations at the guide vane outlet were in a good agreement with the experimental results. The dynamic strain amplitude obtained from the simulations was consistent with the experimental results.

Prototype measurements are costly. Therefore, few results are published in the literature but their detailed results are valuable. The majority of published studies are on strain measurements on the runner blades and on pressure measurements in the draft tube. There are no published investigations on simultaneous pressure and strain measurements on the blades and shaft during the start-up operation of a prototype Kaplan turbine. Such measurements are of interest to correlate the flow acting on the runner blade with its effect on the remaining rotating and stationary domains. This information may help assess the condition in which the runner operates by performing relatively simple measurements on the shaft. Furthermore, the runner blade movement during the start-up operation can be optimized to reduce the pressure fluctuation on the runner blades. In this study, the start-up operation of the prototype Kaplan turbine, Porjus U9, was experimentally investigated. Unsteady pressure and strain measurements were performed on the runner blade, and axial, bending and torsional strain measurements were performed on the shaft. The strain and pressure fluctuations, particularly at low frequency, are discussed during different sequences of the start-up.

2. Experimental Setup and Instrumentation

2.1. Prototype Turbine Description

This study was carried out on the Porjus U9 Kaplan turbine prototype, which belongs to the Porjus Hydropower Center located in the old Porjus hydropower plant on the Lule River. This turbine features a runner with a diameter of 1.55 m and six blades. The runner is located approximately 7 m below the tailwater. The penstock has a total length of approximately 67.1 m with three elbows. The diameter of the penstock varies between 10.5 m at the penstock inlet and 2 m before the spiral case inlet. The draft tube length is approximately 11 m. The rated rotational speed and net head are 600 rpm and 55.5 m, respectively. The distributor has 18 unequally distributed stay vanes and 20 equally spaced guide vanes. The rated output power and flow discharge are 10 MW and 10 m^3s^{-1}, respectively.

2.2. Instrumentation

Different types of transducers were installed on the rotating and stationary components of the turbine. Figure 1 shows the schematic view of the turbine as well as the location and view of two rotating slave chassis on the shaft. A brief description of the installed transducers and data acquisition system is provided here. Additional details on the transducer installation on the blade and data acquisition system are provided in [28].

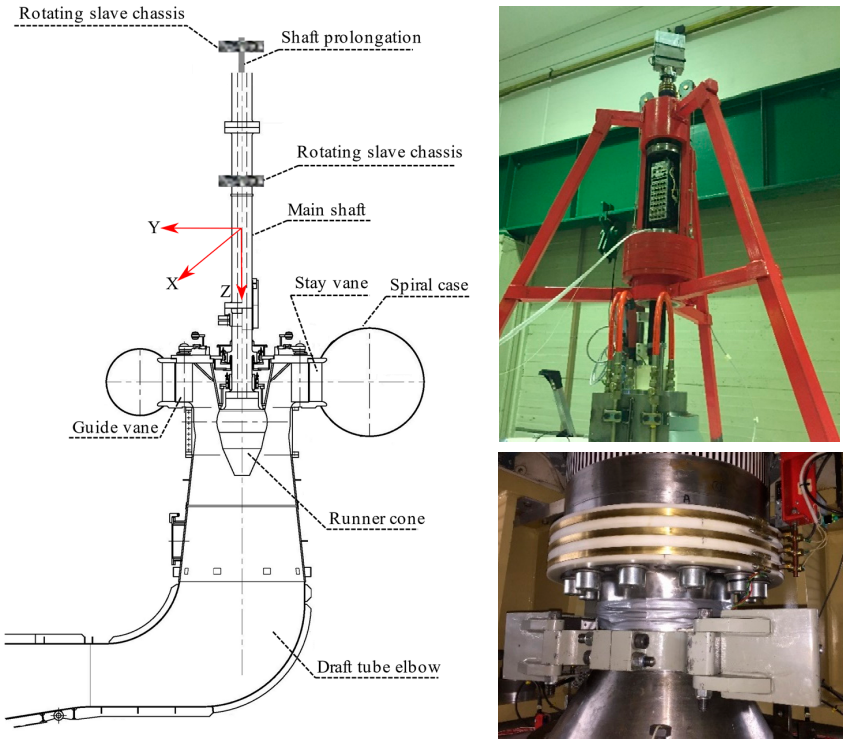

Figure 1. Prototype Kaplan turbine (Porjus U9) schematic and the location of two rotating slave chassis (**left**), rotating slave chassis installed at the top of the shaft (**right-top**) and rotating slave chassis installed on the shaft between the generator guide bearing and turbine guide bearing (**right-bottom**).

2.3. Measurement on the Runner Blade

Miniature piezo-resistive pressure transducers (Kulite LL-080 series) were used. Six pressure transducers were installed on the pressure side (P-PS-1–P-PS-6) and six on the suction side (P-SS-1–P-SS-6) of one runner blade. The first letter in the transducer name stands for 'Pressure', and the second part shows the location of the measurements, e.g., blade pressure side (PS) or suction side (SS). The transducers were located at the intersection of imaginary circles that pass through 1/3 and 2/3 of the

blade's span and 1/4, 1/2 and 3/4 of the blade's chord lines. According to the preliminary finite element analysis, three points were selected on the blade for mounting strain gauges; one strain gauge was mounted close to the leading edge, the second one was mounted near the runner blade hub, and the third one was mounted close to the trailing edge. Two uniaxial strain gauges (K-LY41-6/350-3-2M manufactures by HBM) were installed at each point in the radial and tangential directions on the pressure and suction side. Thus, 12 uniaxial strain gauges were installed on the blade. The transducer S-SS-1T corresponds to the strain measured on the blade suction side at point 1 in the tangential direction. Figure 2 shows the location of pressure transducers and strain gauges on the runner blade pressure side.

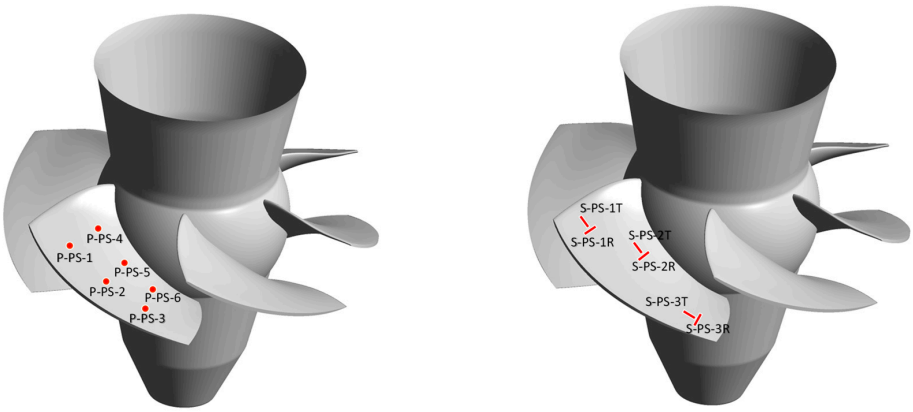

(**a**) (**b**)

Figure 2. Position of the installed transducers on the runner blade pressure side, (**a**) pressure transducers and (**b**) strain gauges.

The uncertainty analysis for the pressure transducers and strain gauges (installed on the runner blade and shaft) was performed using six nonconsecutive repeated measurements at the part load operating point (44.5% guide vane opening). Although there was a deviation in the guide vane opening (approximately 1.3%) and runner blade angle (approximately 0.6°) in the repetitions, only a maximum relative variation of approximately 10% was observed between the standard deviations of individual pressure transducers. The uncertainty for P-PS-2, P-PS-3, P-PS-4, P-PS-6, P-SS-3 and P-SS-4 was estimated to be approximately 0.05%, 0.14%, 0.06%, 0.05%, 0.02% and 0.06%, respectively. The maximum uncertainty of 0.01% was calculated for the strain gauges installed on the runner blade and the shaft.

2.4. Measurement on the Shaft

A total of six strain gauges were installed to the shaft surface between the generator guide bearing and turbine guide bearing. Four uniaxial strain gauges (K-LY41-6/350-3-2M manufactures by HBM) were installed in the axis direction with a 90° spacing for axial and bending strain measurements. This configuration allows us to individually calculate the axial strain and bending strain in the X and Y directions. The rotating coordinate system on the shaft was defined in such a way that the runner rotates in the clockwise direction around the Z-axis, as shown in Figure 1. Two torsion strain gauges (K-XY41-6/350-3-2M manufactures by HBM) were mounted on the same shaft section in the axis direction with a 180° spacing.

2.5. Data Acquisition System

The analog signals from the transducers were collected by the data acquisition system composed of two rotating slave chassis, one stationary slave chassis and one master computer. Each slave included a NI cRIO-9014 embedded real-time controller. One of the rotating slave chassis was installed on the

shaft to digitize the signals from the strain gauges installed on the shaft. The other rotating slave chassis was installed on top of the turbine shaft. The pressure transducers and strain gauges on the runner blade were connected to this unit. The stationary slave chassis acquired the turbine operational parameters such as guide vane opening, runner blade opening angle, power output, headwater level and tailwater level from the turbine control room. The signals from an encoder as well as distance transducers, which were installed near the turbine guide bearing to acquire the shaft displacement, were also digitized by the same unit. The encoder signal was digitized by all data acquisition units (DAQ), which allow postmeasurement synchronization. The signals were oversampled at 5 kHz and then digitally downsampled to 2.5 kHz.

3. Data Processing

Transient variation and spectral analysis of the pressure and strain signals were carried out. The time-averaged values of the transient signals were obtained using the Savitzky-Golay method [29]. A polynomial order of two with a frame size of 5 s was selected. The fluctuation component of the signal can be expressed as:

$$\widetilde{X}(t) = X(t) - \overline{X}(t), \quad (1)$$

where $\widetilde{X}(t)$, $\overline{X}(t)$ and $X(t)$ are the fluctuating component of the signal, the time-averaged value of the signal, and the acquired raw signal, respectively. The spectral analysis of the data was carried out using the short-time Fourier transform (STFT) in MATLAB. The fluctuating component of the pressure and strain signals was considered for the spectral analysis. A window size of 11 s with a 95% overlap was selected. The power spectral density obtained from the spectral analysis was modified by the following equation:

$$PSD_{log} = 10 \times \log(10 \times PSD), \quad (2)$$

The obtained frequencies are normalized by the runner rotational frequency. The pressure data are normalized with respect to the initial pressure value in the turbine chamber before filling the waterway (P_{ref}).

The time-averaged normalized peak-to-peak value was calculated by considering 2σ, which holds 95% of the highest peak of the data within the sliding window, to investigate the strain and pressure fluctuation amplitudes during the start-up operation to compare these values to the steady-state operation with a 61% guide vane opening. A sliding window size of 0.1 s was used. The average value of each signal at the steady-state operation was used to normalize the peak-to-peak values.

The transient strain data obtained on the shaft showed an interference of the encoder signal in the rotating slave chassis installed on the shaft. This signal added spikes at a frequency of 10 Hz, which corresponded to the turbine runner rotational frequency. The spikes appeared at the same time for all strain gauges. A Savitzky–Golay filter with a polynomial order of two and a frame size of 0.02 s was applied to the strain data. The values of the spikes were replaced by the filtered values at that location which removed the effect of the encoder signal. By comparing the treated signals with the original signals, it was determined that the time-averaged value obtained by the Savitzky–Golay method was not influenced by these spikes.

4. Results and Discussion

Synchronized pressure and strain measurements were performed on the prototype Kaplan turbine during the start-up operation. Several pressure transducers and strain gauges installed on the runner blade could not deliver reliable data due to malfunctioning. Therefore, only the data of the pressure transducers P-PS-2, P-PS-3, P-PS-4, P-PS-6, P-SS-3 and P-SS-4 and strain gauges S-PS-3R, S-PS-3T, S-SS-4R, S-SS-4T, S-SS-5R, S-SS-5T, S-SS-6R and S-SS-6T will be presented. All strain gauge data from the shaft will be presented. The need to discard some of the sensors indicates the challenging environment in the runner and the need to develop simple and efficient methods to assess the health of the turbine. The variation in the turbine general parameters (e.g., guide vane opening, runner blade angle and

rotational speed) is presented. The detailed analysis of the pressure and strain fluctuations was performed, and the frequency spectral analysis was carried out to assess the frequency development, particularly in the low-frequency region. Four nonconsecutive repeated measurements at the start-up were performed to examine the repeatability of the measurement, and similar results were obtained.

The start-up operation of the Kaplan turbine consists of different stages. Figure 3 shows the variation in the runner blade angle, normalized rotational speed and guide vane opening. The rotational speed and guide vane opening were normalized by the rated rotational speed and the maximum guide vane opening, respectively. During the first stage, t_0, which is called the acceleration phase, the guide vanes were opened from the completely closed position with a prescribed opening rate until the opening limit was reached, i.e., approximately 14% opening. The runner rotational speed increased with an increase in the flow rate. The angle of runner blades decreased from −7° to −17° and remained unchanged until the end of the magnetization phase to further increase the runner angular momentum. The runner blade angle and the guide vane angular opening range of this unit was +10° to −17° and 0–35° (0–100% opening), respectively. The guide vanes remain unchanged for approximately 25 s. When the rotational speed reached the fold back speed (approximately 90–95% of the rated speed), after a slight increase in the guide vane opening, it decreased to fold back opening and remains in this position for 37 s. This stage is called speed-no-load and corresponded to the period t_1 in Figure 3. The synchronous speed was achieved, and there was no significant variation in the runner blade angle and guide vane opening during this phase. During the third stage, t_2, the generator magnetization was initiated, and the guide vanes were automatically opened in a limited range and remained unchanged until t = 120 s, while the runner blades were still at the minimum angle. Thereafter, during the fourth stage, t_3, the guide vane opening increased to the value given by the unit operator (in this case, 61% opening), and the runner blades automatically adjusted to −4.4°. The power output increased by further opening the guide vanes.

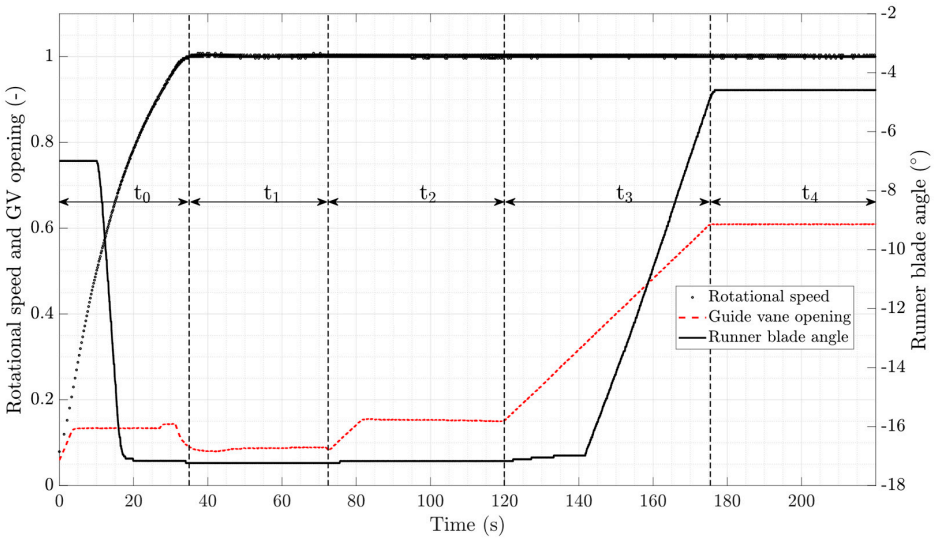

Figure 3. Transient variation of the normalized rotational speed, guide vane opening and runner blade angle during the turbine start-up operation; vertical black dashed lines indicate the different stages of the start-up operation.

Figure 4 presents the variation in the axial strain, torsion strain and bending strain in the X and Y direction on the shaft. The vertical black dashed lines divide each stage of the start-up operation. In the first stage, three peaks can be observed in the axial strain. The axial strain increases by opening the guide vanes, and the first peak occurs when the guide vane opening reaches the opening limit at t = 3 s. Thereafter, the axial strain decreases because the blade angle and guide vane opening are constant and the pressure difference between the blade pressure and suction side decreases. By decreasing the

runner blade angle, the axial strain is increased and the second peak occurs at approximately t = 18 s where the blade angle reaches the minimum value. This outcome occurs because the projected area of the runner increases by closing the runner blades. Then, the runner accelerates, and the strain decreases as the flow stabilizes with the constant guide vane opening and runner blade angle. A small variation in the strain is observed by changing the guide vane opening at the end of the first stage. During the second and third stages (i.e., speed-no-load and generator magnetization, respectively), the axial strain follows the movement of the guide vanes because the runner blade angle is fixed. This continues during the fourth stage until the runner blade angle increases, which decreases the axial load on the runner. This outcome shows that the axial strain on the shaft is directly proportional to the guide vane opening and inversely proportional to the blade angle. The minimum axial strain is obtained under the speed-no-load condition. Similar to the axial strain, the time-averaged torsion strain variation follows the guide vane opening except for the first stage, as the rotational speed of the turbine is not at the rated speed. The torsion strain is increased in the beginning by opening the guide vanes as the shaft startes to rotate from a still position. Then, the torsion strain is decreased by increasing the rotational speed where it reaches the synchronous speed at the end of the first stage. The minimum torsion strain is obtained during the speed-no-load phase at approximately 10 μm/m because there is no power extracted from the generator. This value mainly reflects the losses in the turbine bearings and ventilation losses in the generator. The variation of the time-averaged bending strain in the X and Y directions follows the guide vane opening in all stages except for the first stage as the runner blade angle is also changed. The bending strain increases in magnitude by increasing the guide vane opening and decreases by lowering the opening. The bending strain in both directions instantly increases by opening the guide vane from the completely closed position. Then, it is decreased until the end of the first stage. This outcome shows that the lateral forces acting on the runner blade are high at the beginning of the start-up phase compared to those during the speed-no-load condition, which indicates a nonsymmetrical flow.

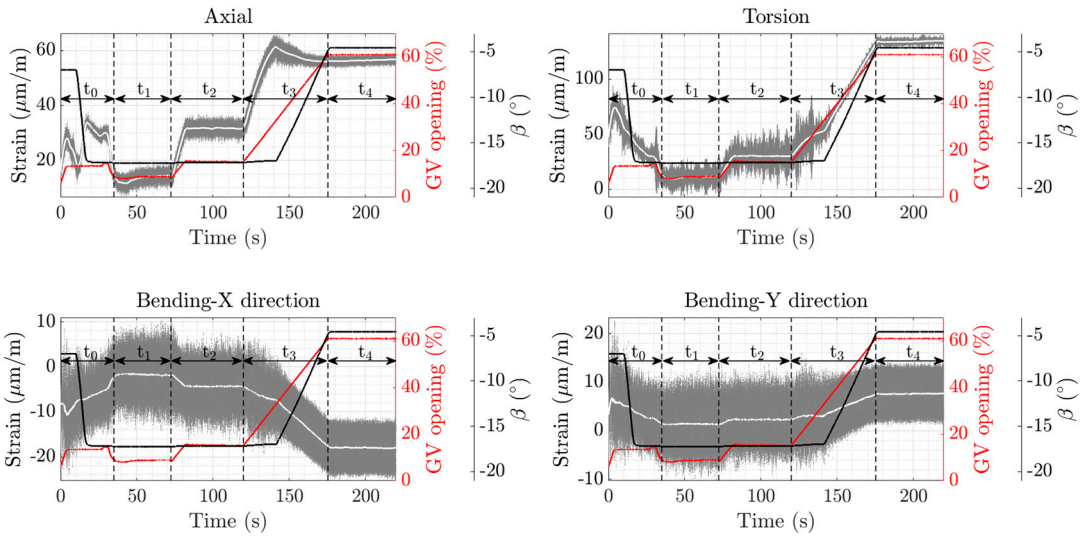

Figure 4. Transient variation of the axial, torsion and bending strain in the X direction, and bending strain in the Y direction during the turbine start-up operation; gray dots: instantaneous strain; white line: time-averaged strain; red line: guide vane opening; black line: runner blade angle; vertical black dashed lines indicate different stages of the start-up operation.

Figure 5 shows the transient variation of the normalized peak-to-peak value of the axial strain, torsion strain and bending strain in the X and Y directions on the shaft. The strain peak-to-peak values were normalized using the average value of each strain data obtained during the steady-state operation reached at the end of the transient. The average peak-to-peak value of axial strain, torsion strain and bending strain in the X and Y directions in the steady-state operation are 1.25, 2.80, 7.40 and 7.06 μm/m,

respectively. Large variations in the normalized peak-to-peak value are observed in the torsion strain compared to the axial and bending strains. A high peak is observed at the end of the first stage during a small change in the guide vane opening before reaching the speed-no-load phase. The peak-to-peak value gradually increases after magnetization and reaches the maximum value at t = 133 s, which is approximately 12 times that of the steady-state, when the guide vanes opening increases and the runner blades are still at the minimum angle. The level of the strain fluctuation amplitude is considerably lowered after adjusting the runner blade angle at t = 150 s. No significant bending strain fluctuations in the X and Y directions are observed during the start-up compared to the steady-state operation. The axial strain fluctuation level decreases by decreasing the runner blade angle during the first phase of the start-up. A constant level of fluctuation is observed during the speed-no-load and generator magnetization phases. Then, it slightly increases by further opening the guide vanes as the runner blades are at the minimum opening. Thereafter, it reaches the minimum level as the runner blade angle is adjusted.

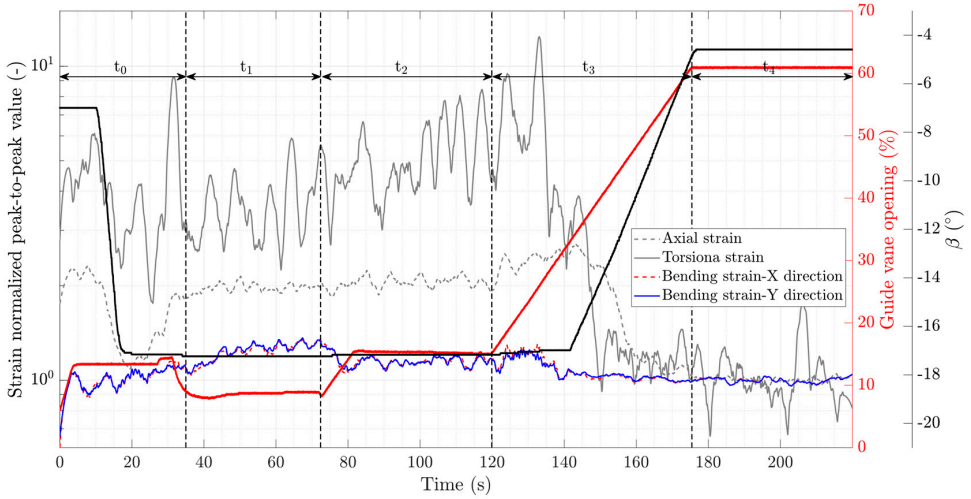

Figure 5. Transient variation of the normalized peak-to-peak value of axial, torsion, bending in the X direction and bending in the Y direction strain during the turbine start-up operation; red line: guide vane opening; black line: runner blade angle; vertical black dashed lines indicate the different stages of the start-up operation.

Figure 6 shows the power spectra of the axial strain data obtained from the shaft during the start-up operation. Low-frequency fluctuations are observed in the normalized frequency range of 0–1.5 (0–15 Hz) at the beginning of the start-up, 0–10 s. The runner blade angle is constant, −7°, and guide vanes are opened from the closed position to 14%. The low guide vane angle creates a large swirling flow in the vaneless space with recirculation, which might be the cause of these high random fluctuations. High shear flow and turbulence level occurs during low guide vane opening and runner blade angle. A dominant normalized frequency of 2 is observed in the spectrogram, which appears when the runner rotational speed is close to the synchronous speed, at t = 30 s. This dominant frequency might be attributed to the runner blade configuration consisting of two runner blades; one blade was instrumented with transducers, and the other blade with only an epoxy to balance the runner. Except for this frequency, no significant dominant frequency in the low-frequency region is observed during the speed-no-load operation. A dominant normalized frequency appears after generator loading ($f_n = 0.93$), t = 80–120 s; the frequency varies by changing the guide vane opening and runner blade angle. Later, one can see this dominant frequency in the pressure data on the runner blade pressure side and strain results on the runner blade. Houde et al. [30] reported a dominant frequency below the runner rotational frequency ($f_n = 0.88$), which results from the rotating stall being linked to vortical flow structures in the vaneless space at speed-no-load. The number of these

structures can be altered by the guide vane opening, as described in [31], which can result in different dominant frequencies. The dominant frequency and energy intensity slightly increase at t = 120–150 s. The variation of this dominant frequency is accompanied by the variation of another low frequency (approximately $f_n = 0.12$) at the same time period but in the opposite direction, which indicates a coupling between them.

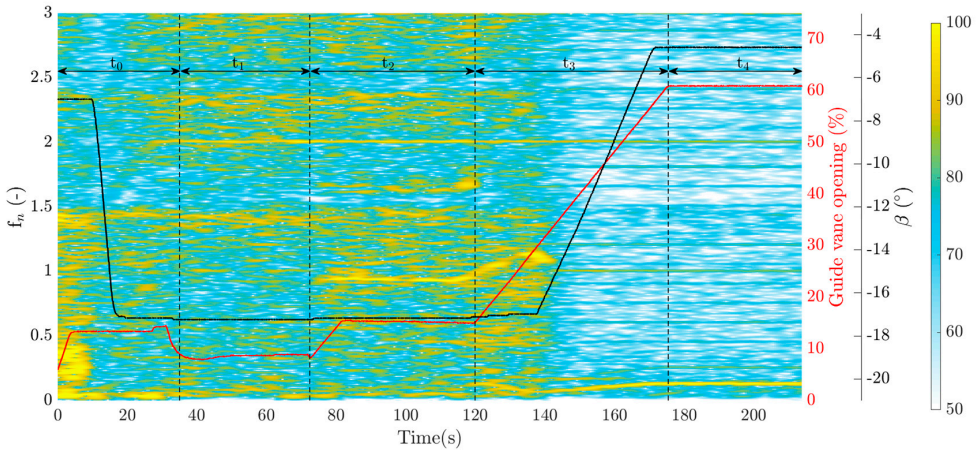

Figure 6. Spectrogram of the axial strain data from the shaft during the turbine start-up operation; vertical black dashed lines indicate the different stages of the start-up operation; red line: guide vane opening; black line: runner blade angle.

The frequency spectra of the torsion strain data obtained from the shaft are shown in Figure 7. Most of the energy in the spectrogram is accumulated around the region within $f_n = 2.5$–4. These fluctuations start from the beginning of the start-up and continues until t = 140 s, where the runner blade angle is adjusted by the governor according to the given guide vane opening. Thereafter, the high-intensity region narrows and appears around $f_n = 3.2$. This frequency corresponds to the first torsional mode of the shaft. Similar to the axial strain spectrogram, the low-frequency fluctuations are observed at the beginning of the start-up until t = 15 s. Similar to the bending strain spectrogram, an evolving dominant frequency could be seen that follows the runner rotational frequency and reaches $f_n = 1$ at the end of the acceleration phase. Dominant frequencies of $f_n = 0.93$ and $f_n = 2$ are observed in the torsion strain spectrogram starting in the speed-no-load phase and loading the generator, respectively. These frequencies appear in the axial strain at different times; $f_n = 0.93$ appears during the generator magnetization phase and $f_n = 2$ appears at the end of the acceleration phase. Similar to the axial strain results, the dominant frequency of $f_n = 0.93$ changes with the guide vane and runner blade movement at t = 120 s. As observed in the axial strain spectrogram in Figure 6, the variation of this dominant frequency is accompanied by another low frequency, approximately $f_n = 0.12$. In addition, $f_n = 1.6$ is observed during t_2 when the generator is loaded. This frequency could be attributed to the magnetic stiffness and the stiffness of the stator considering a rigid body motion.

Figure 8 presents the spectrogram of the bending strain on the shaft in the X-direction. In the low-frequency region, the bending strain fluctuations have an evolving dominant normalized frequency increasing from 0.2 to 1 during the acceleration phase. The dominant normalized frequency of $f_n = 1$ could be seen after reaching the synchronous speed at t = 35 s. A high-intensity region is observed around $f_n = 3.2$ from the beginning of the start-up until t = 140 s when the runner blades were opened from the minimum angle. This observation indicates a coupling between the twisting (torsional) and the bending motion of the runner. Another dominant frequency ($f_n = 0.88$) appears for a short period of time, at t = 120–140 s, when the runner blades are slightly opened. Another high-intensity region is observed around $f_n = 2.5$ during the generator loading, t_2. A similar frequency content is observed for the bending strain in the Y direction. Therefore, it is not presented.

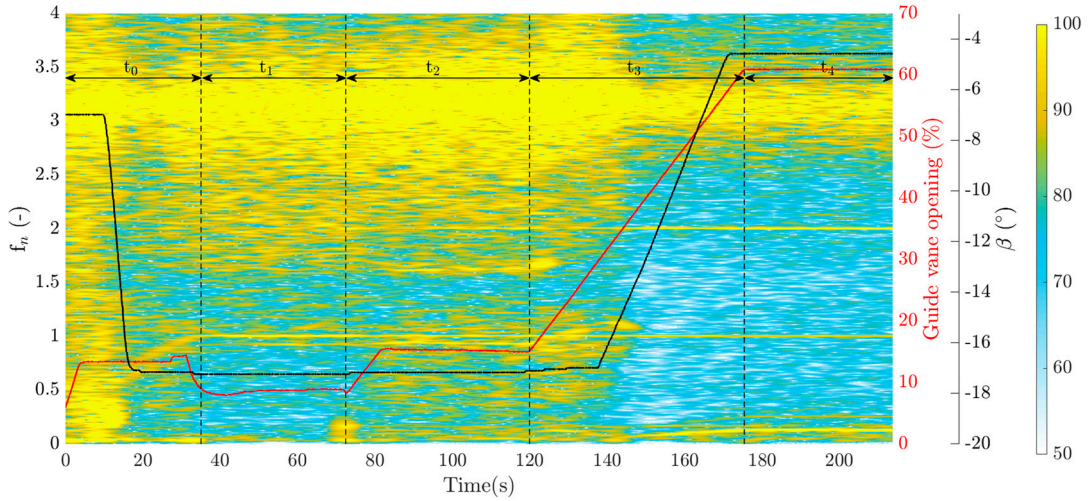

Figure 7. Spectrogram of the torsion strain data from the shaft during the turbine start-up operation; vertical black dashed lines indicate the different stages of the start-up operation; red line: guide vane opening; black line: runner blade angle.

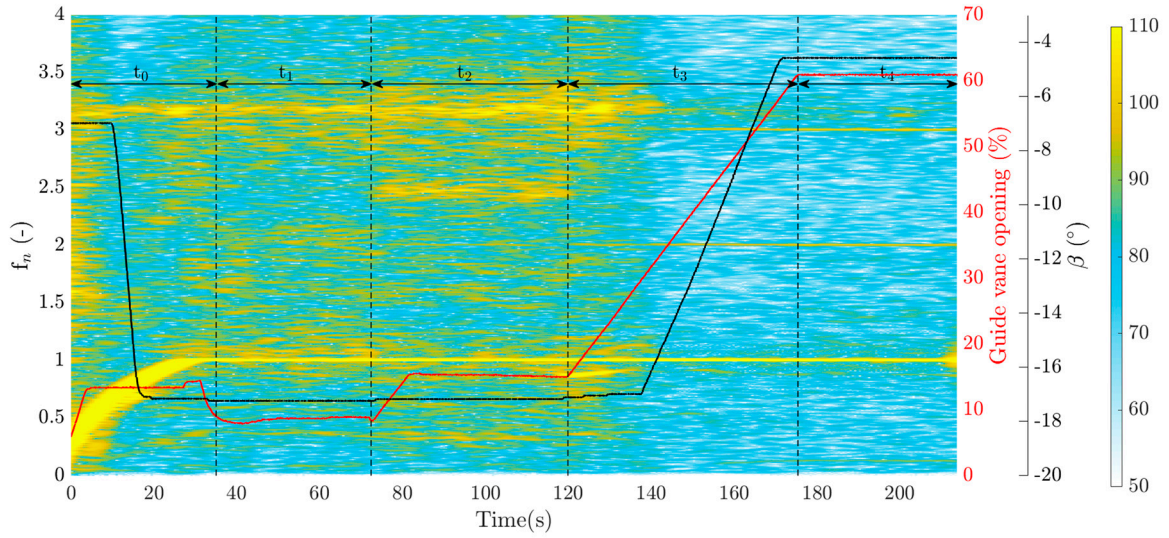

Figure 8. Spectrogram of the bending strain data in the X direction from the shaft during the turbine start-up operation; vertical black dashed lines indicate the different stages of the start-up operation; red line: guide vane opening; black line: runner blade angle.

Figure 9 presents the normalized pressure variation on the runner blade for six pressure transducers. Regardless of the normalized pressure values, a similar qualitative behavior is obtained for the transducers on the blade pressure side (P-PS-2, P-PS-3, P-PS-4 and P-PS-6) and S-SS-4 installed on the suction side. However, the pressure variation for the pressure transducer S-SS-3 is different and remains constant up to the end of the third phase (end of the magnetization phase), t = 120 s. Thereafter, the normalized pressure value slightly decreases by increasing the guide vane opening as well as the runner blade angle, and high amplitude fluctuations are captured around t = 160 s.

Figure 10 shows the pressure normalized peak-to-peak variation for the pressure transducers on the runner blade. The pressure peak-to-peak values were normalized using the average value of each pressure data during the last phase of the operation (steady-state operation). The average pressure peak-to-peak values of 0.075, 0.081, 0.066, 0.081, 0.030 and 0.080 were obtained during the steady-state operation for P-PS-2, P-PS-3, P-PS-4, P-PS-6, S-SS-3, and S-SS-4, respectively. High amplitude fluctuations are captured for all the pressure transducers at the beginning of the start-up operation

by opening the guide vanes while the runner blade angle is approximately −7°. These fluctuations are approximately 3–7 times larger than those during the steady-state operation. Closing the runner blades, while the guide vanes opening is fixed, temporarily decreases pressure fluctuations on the runner blade during the acceleration phase. No significant changes are observed for the pressure fluctuations from the speed-no-load stage to the end of the magnetization stage, t = 120 s. Thereafter, the fluctuation level considerably decreases for all pressure transducers except for S-SS-3 by opening the guide vane and runner blades around t = 145 s. A large peak is observed at t = 165 s for S-SS-3, which is more than 10 times larger than those during the steady-state operation.

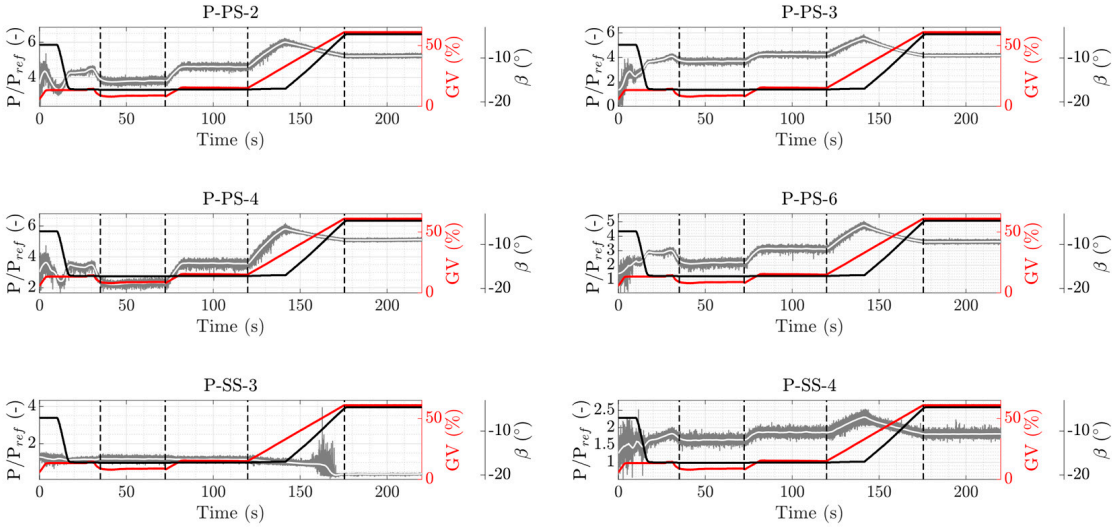

Figure 9. Transient normalized pressure variation on the runner blade during the turbine start-up operation; vertical black dashed lines indicate the different stages of the start-up operation; red line: guide vane opening; black line: runner blade angle.

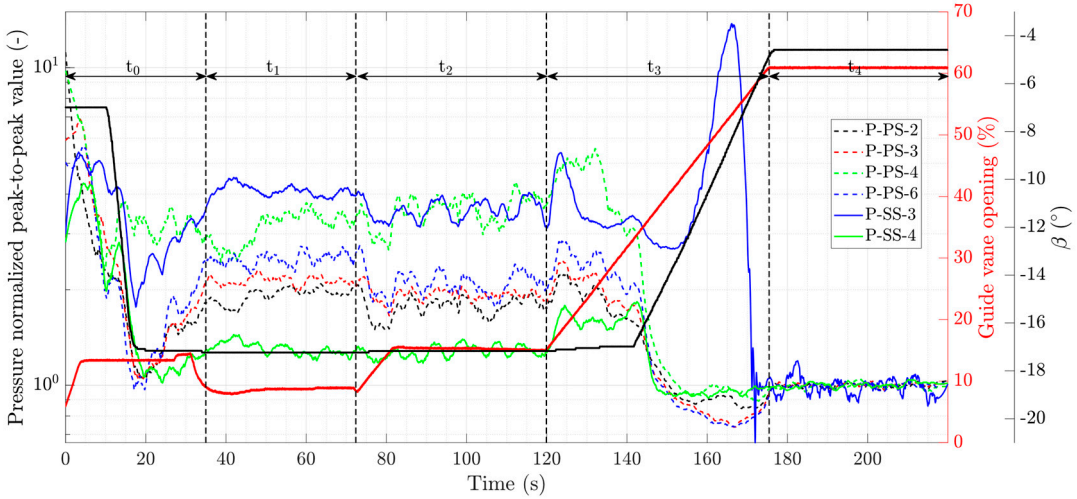

Figure 10. Transient variation of the pressure normalized peak-to-peak value during the turbine start-up operation; red line: guide vane opening; black line: runner blade angle; vertical black dashed lines indicate the different stages of the start-up operation.

Figure 11 shows the spectrogram of the pressure transducer P-PS-4 during the start-up. The frequency content of other pressure transducers installed on the pressure side is similar; therefore, they are not presented. Two main evolving dominant frequencies are observed in the frequency spectrum reaching the final value at the beginning of the speed-no-load stage; the runner frequency is $f_n = 1$ and the other frequency is $f_n = 0.93$ (Figure 11a), which was also observed in the axial

and torsion strain on the shaft, as shown in Figures 6 and 7. By loading the generator and opening the guide vanes, the energy of the runner frequency decreases. However, the intensity of the other frequency ($f_n = 0.93$) increases, and the dominant frequency value increases after t = 120 s by further opening the guide vanes. This outcome was also observed in the strain data obtained from the shaft. Low-frequency fluctuations ($f_n < 1$) are captured in all pressure transducers installed on the blade pressure side at the beginning of the start-up, t = 0–10 s, and considerably decrease by reducing the runner blade angle. Figure 11b shows the frequency content within the expected RSI frequency region, approximately $f_n = 20$. No dominant frequency is observed during the start-up operation. The RSI frequency appeares at t = 150 s when the guide vane opening reaches approximately 45%. Clearly, the wakes of the guides are either weak or not developed enough to reach the runner blades.

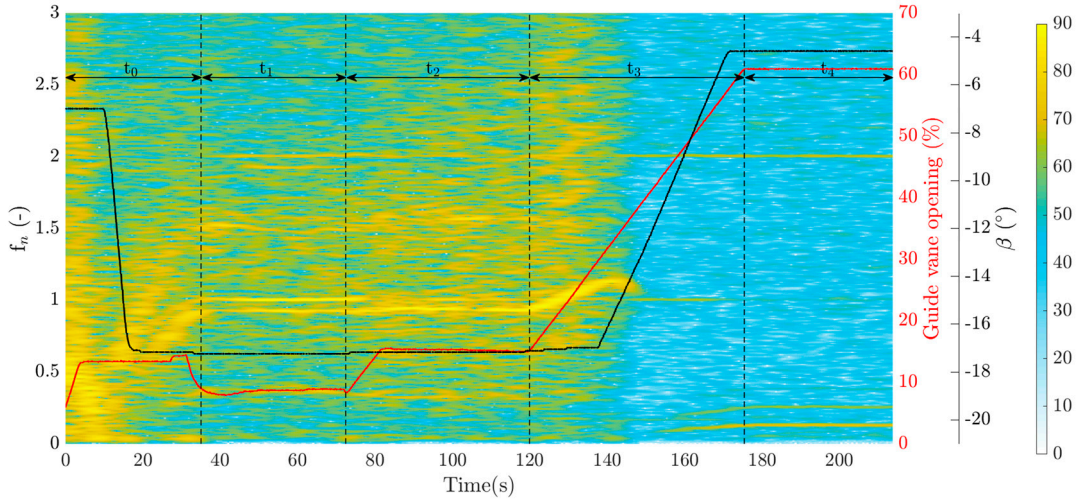

(**a**)

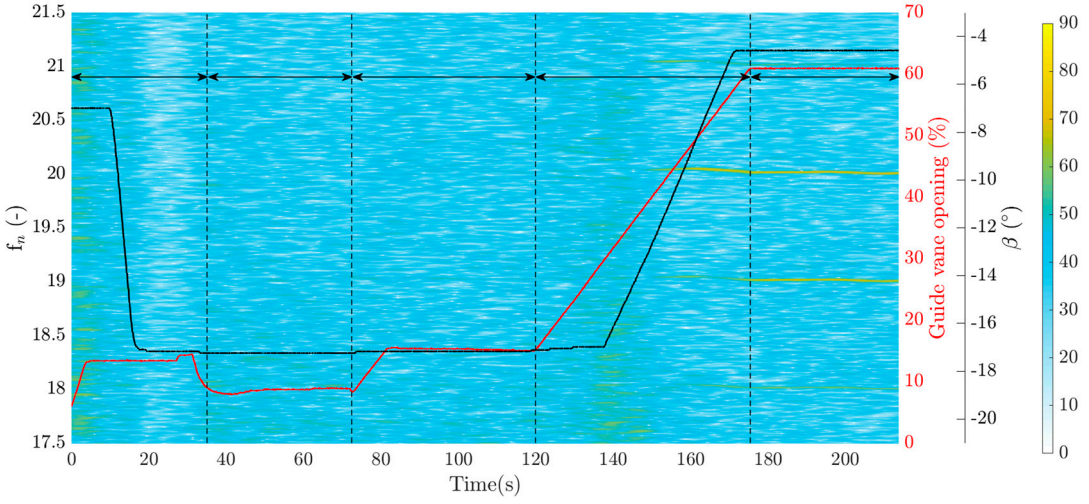

(**b**)

Figure 11. Spectrogram of the pressure transducer P-PS-4 (installed on the runner pressure side leading edge close to the hub) during the turbine start-up operation: (**a**) low-frequency range (f_n = 0–3) and (**b**) frequency range of f_n = 17.5–21.5; vertical black dashed lines indicate the different stages of the start-up operation; red line: guide vane opening; black line: runner blade angle.

Figure 12 shows the spectrogram of the pressure transducer S-SS-4 during the start-up. The runner frequency is only captured during the speed-no-load stage. Similar to P-PS-4, low-frequency fluctuations

($f_n < 1$) are observed at the beginning of the start-up. No dominant frequency is detected during the magnetization of the generator in this range. By further opening the guide vane, the varying dominant frequency appears and is similar to P-PS-4 at t = 120–140 s.

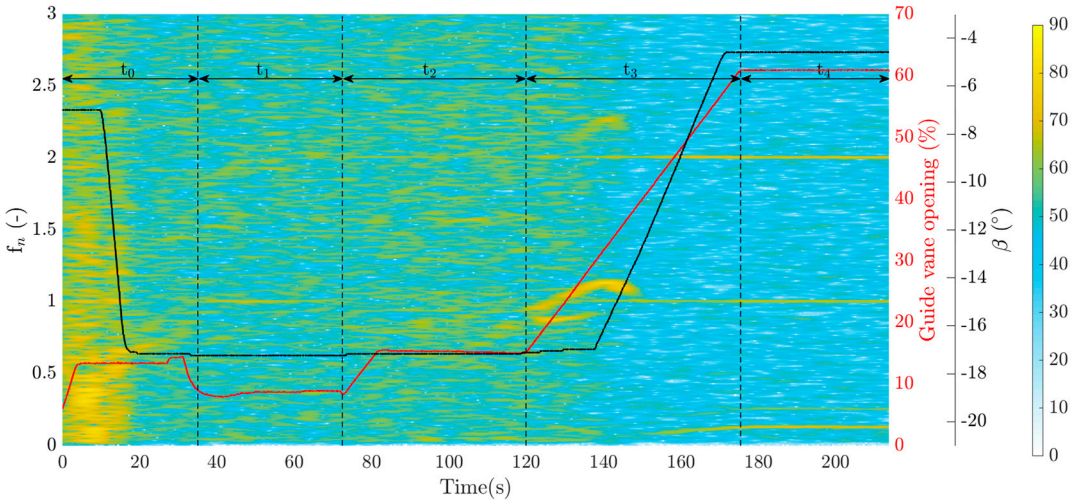

Figure 12. Spectrogram of the pressure transducer P-SS-4 (installed on the runner suction side leading edge close to the hub) during the turbine start-up operation; vertical black dashed lines indicate the different stages of the start-up operation; red line: guide vane opening; black line: runner blade angle.

The transient strain data obtained from the runner blade are shown in Figure 13. The strain gauges installed on the runner blade pressure side close to the trailing edge (S-PS-3R and S-PS-3T) experience an increasing strain during the start-up operation as the guide vanes are opened from the closed position. The strain in the radial direction (S-PS-3R) slightly decreases by opening the runner blades at t = 140 s, whereas the guide vanes are further opened. The strain value close to the blade leading edge in the tangential direction (S-SS-4T) has the maximum value at the beginning of the start-up and then gradually decreases by lowering the runner blade angle during the acceleration phase. The strain value remains rather unchanged after the turbine reaches the synchronous speed. However, the strain value at S-SS-4R is rapidly changed from +50 to −150 µm/m by decreasing the runner blade angle during the first stage of the start-up. Then, the strain values follow the guide vane movement regardless of the runner blade movement. As expected, the strain gauges installed close to the hub (S-SS-5R and S-SS-5T) experience higher strain values than those at other locations that reach approximately −500 µm/m . The stochastic behavior of the time-averaged strain value could be observed for strain gauges installed close to the blade hub and trailing edge on the suction side at t = 0–120 s.

The fluctuating component of the strain on the runner blades is an important parameter to investigate the fatigue life of a turbine. To compare the fluctuation level of the strain signals, the normalized peak-to-peak values are presented in Figure 14. The strain peak-to-peak values were normalized using the average value of each strain data during the last phase of the operation (steady-state operation). The average strain peak-to-peak values of 13.78, 14.96, 8.53, 7.08, 46.74, 108.05, 37.93 and 20.99 µm/m are obtained during the steady-state operation for S-PS-3R, S-PS-3T, S-SS-4R, S-SS-4T, S-SS-5R, S-SS-5T, S-SS-6R and S-SS-6T, respectively. After reaching the synchronous speed, the peak-to-peak values for all strain gauges, except for the ones installed close to the blade leading edge (S-SS-4R and S-SS-4T), have almost the same order of magnitude as those during the steady-state operation. Large peaks are observed for S-SS-4R and S-SS-4T around t = 135 s during the guide vane opening when the runner blades are rather fixed. Similar to the pressure results shown in Figure 10, the peak-to-peak values first increase by opening the guide vanes and then decrease by opening the

runner blades for all strain gauges as the guide vane and runner blade angle matche to achieve a smoother operation.

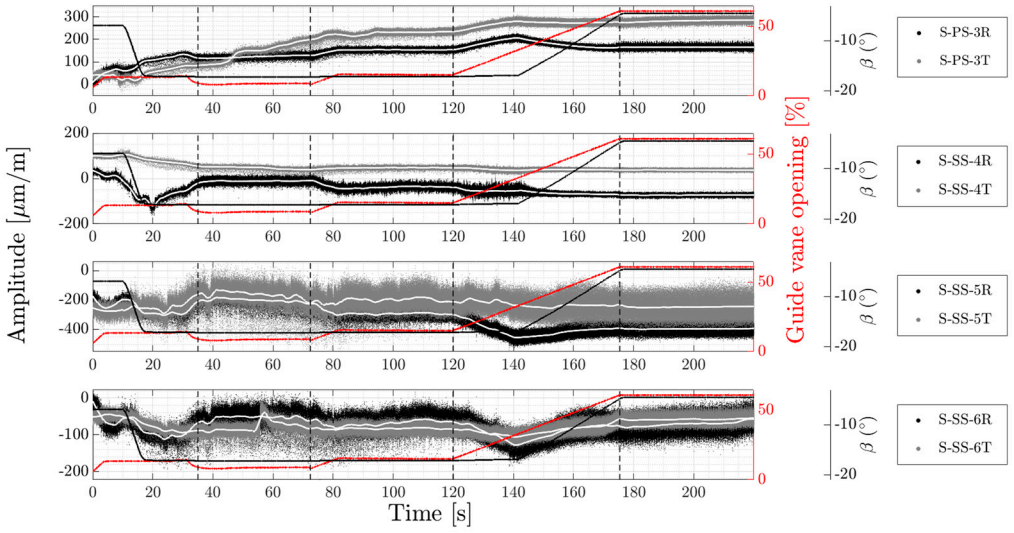

Figure 13. Transient variation of strain on the runner blade during the turbine start-up operation; dots: instantaneous strain; white line: time-averaged strain; red line: guide vane opening; black line: runner blade angle; black line: runner blade angle; vertical black dashed lines indicate the different stages of the start-up operation.

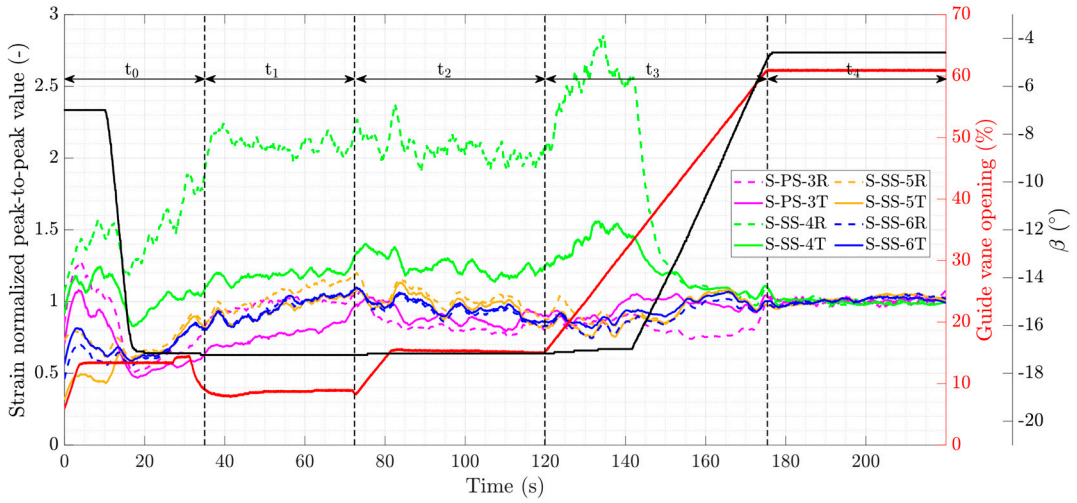

Figure 14. Normalized peak-to-peak value of strain fluctuations on the runner blade during the turbine start-up operation; red line: guide vane opening; black line: runner blade angle; vertical black dashed lines indicate the different stages of the start-up operation.

Four strain gauges were selected on the blade suction side to analyze the frequency content of their signals; two strain gauges were close to the blade leading edge, and the other two were close to the blade hub. Figure 15 shows the time-frequency plots of strain gauges S-SS-4R and S-SS-4T. The color bar range is slightly different for the subfigures. A dominant normalized frequency ($f_n = 1$) is observed for both strain gauges starting at the end of the acceleration phase. The dominant varying frequency is clearly seen for both strain gauges between t = 120 s and t = 140 s, which was previously observed for pressure sensors in Figures 11a and 12. The main difference between the frequency spectrograms of the strain gauges in the radial and tangential direction at this location is the appearing time of the dominant normalized frequency of $f_n = 0.93$ and $f_n = 2$. The dominant frequency of $f_n = 0.93$ appears

at the beginning of the magnetization phase for the strain gauge S-SS-4T, whereas it only appears for a short time, t = 50–70 s in the speed-no-load for the strain gauge S-SS-4R. The dominant frequency of $f_n = 2$ could be observed from the beginning of the fourth stage for S-SS-4R, while it appears in the speed-no-load for S-SS-4T.

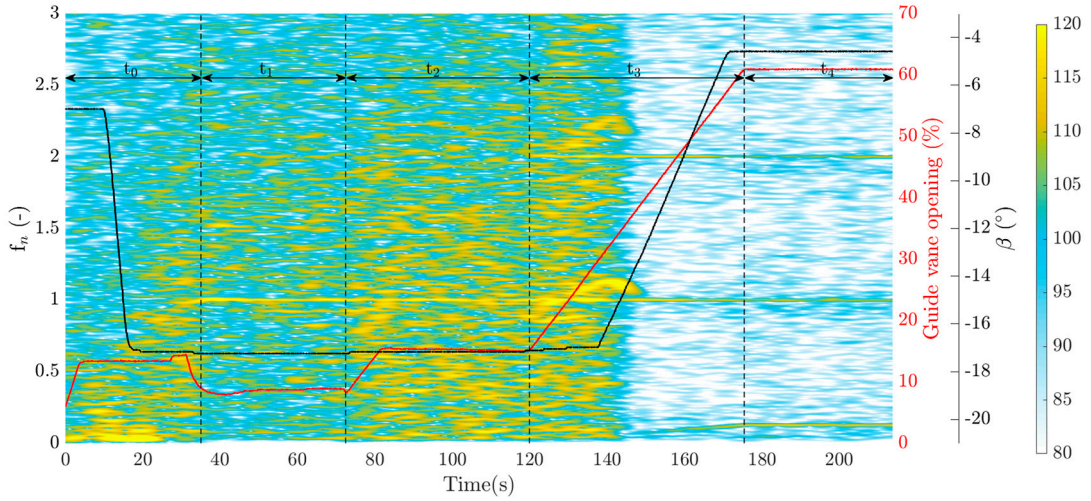

(**a**)

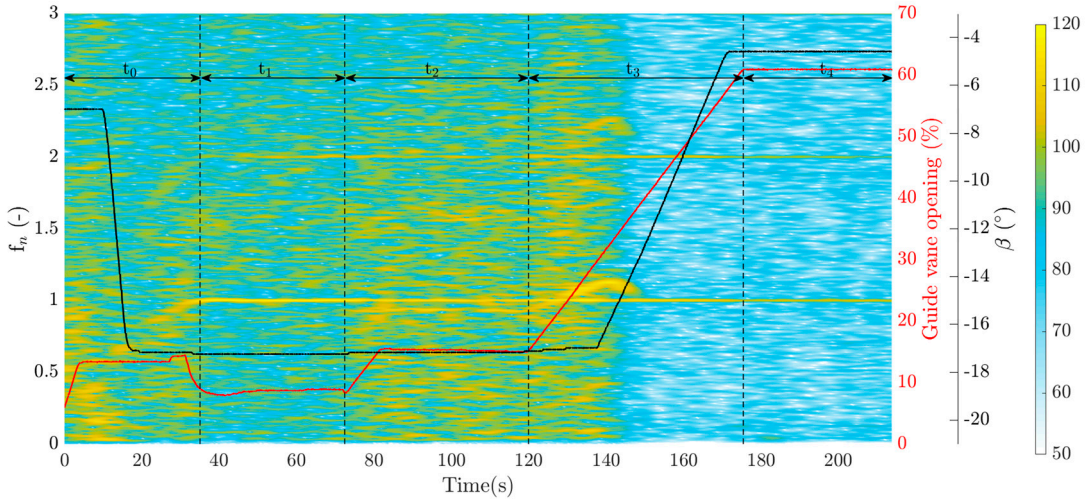

(**b**)

Figure 15. Spectrogram of the strain data on the runner blade during the turbine start-up operation. (**a**) S-SS-4R strain gauge and (**b**) S-SS-4T strain gauge; vertical black dashed lines indicate the different stages of the start-up operation; red line: guide vane opening; black line: runner blade angle.

Figure 16 shows the spectrogram of the strain gauges S-SS-5R and S-SS-5T during the start-up. A varying dominant normalized frequency (reaching $f_n = 1$) and its harmonics are observed for both strain gauges reaching their final value at the end of the acceleration phase. The dominant normalized frequency of $f_n = 0.93$ could be only seen for S-SS-5R appearing in the speed-no-load, approximately t = 50 s. This outcome indicates a fluid phenomenon that is initially oscillating in the radial direction close to the hub (S-SS-5R), at t_1, and then in the circumferential direction in the leading edge (S-SS-4T), at t_2. A dominant frequency of $f_n = 2.5$ and its harmonics are also observed for both strain gauges. This frequency could be attributed to the blade's fundamental mode.

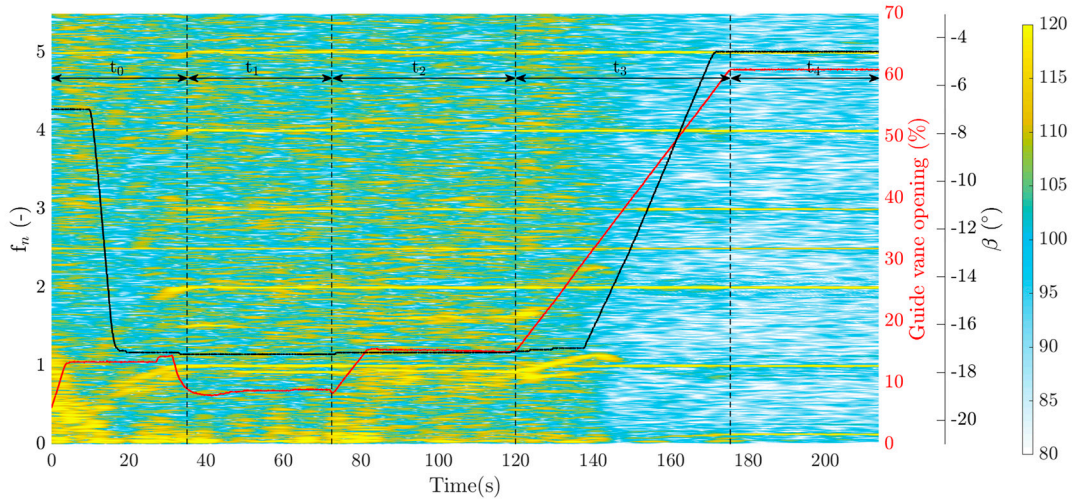

(**a**)

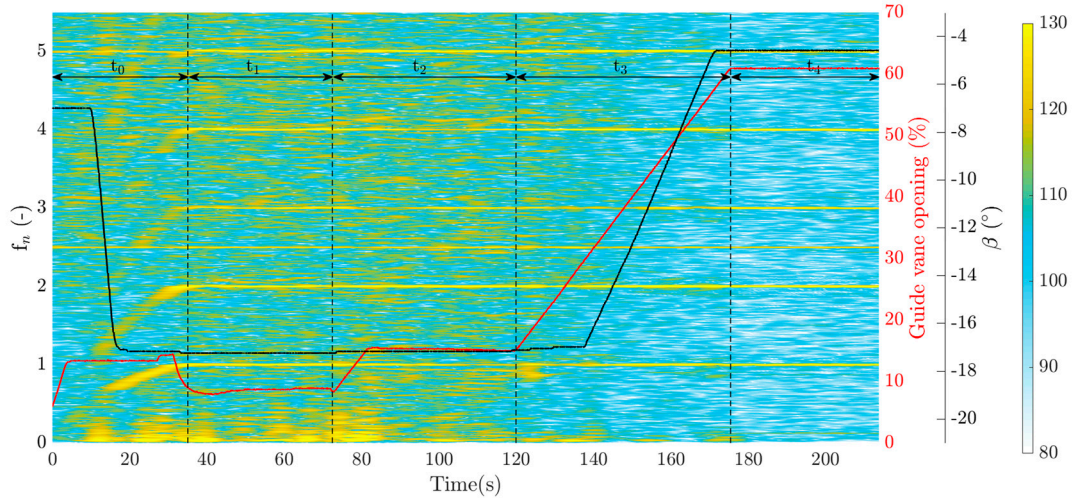

(**b**)

Figure 16. Spectrogram of the strain data on the runner blade during the turbine start-up operation. (**a**) S-SS-5R strain gauge and (**b**) S-SS-5T strain gauge; vertical black dashed lines indicate the different stages of the start-up operation; red line: guide vane opening; black line: runner blade angle.

5. Conclusions

The start-up operation of the prototype Kaplan turbine was experimentally investigated. The synchronized unsteady pressure and strain measurement on the runner blade and strain measurement on the shaft were performed. The measurement on the shaft consisted of axial, torsion and bending strain measurement. The strain gauges on the blade were installed in the radial and tangential direction. The instrumentation and data acquisition system were briefly mentioned. The general parameters of the turbine (e.g., runner rotational speed, guide vane opening, and runner blade angle) were also acquired to differentiate each phase of the start-up operation. The guide vane opening value and runner blade angle were automatically adjusted by the governor from the beginning of the operation until the end of the generator magnetization. The runner rotational speed increased almost exponentially during the first phase.

The strain measurement on the shaft showed that the axial, torsion and bending strains followed the guide vane opening during the start-up except for the first phase where the runner blade angle

simultaneously changed with the guide vane opening. The axial strain data showed that the projected area of the runner blades directly affected the axial strain in the shaft. The bending strain peak-to-peak value in the X and Y directions was almost three times larger than the axial strain fluctuation. This outcome may cause problems in the turbine bearing due to the non-uniform load distribution. Large variations of the normalized peak-to-peak value were observed in the torsion strain compared to the axial and bending strains. A large torsion strain fluctuation was observed close to the speed-no-load phase, which was approximately nine times that of the steady-state operation; the fluctuation amplitude gradually increased from the second phase, and another large peak (approximately 12 times that of the steady-state operation) was obtained at the beginning of the last phase at t = 133 s, where the guide vane opening increased and the runner blade angle was still at the minimum angle. The runner normalized frequency, its second harmonic, and $f_n = 0.93$ appeared in the axial and torsion strain data. In addition, a varying dominant frequency ($f_n = 0.93$–1.14) was obtained at the end of the magnetization phase for approximately 20 s, which was also observed in the pressure and strain data on the runner blade. A high-intensity region was observed in the spectrogram of the torsion data within $f_n = 2.5$–4 appearing at the beginning of the start-up. The frequency band became narrow after increasing the load at t = 140 s.

High amplitude fluctuations were captured for all pressure transducers at the beginning of the start-up operation. No significant changes were observed for the pressure fluctuations from the speed-no-load stage to the end of the magnetization stage. A high fluctuation level was obtained for the pressure transducer installed close to the shroud at the trailing edge during the load increase at t = 165 s. The RSI frequency was not detected for the pressure transducers during the start-up operation. It was shown that the guide vane opening has to reach a certain level (approximately 45%) to observe the RSI frequency. The strain measurement on the runner blade showed that not only a higher strain but also a higher strain fluctuation occurred at the location close to the blade hub.

Author Contributions: A.S.D. performed the experiments, analyzed the data, and prepared the manuscript. F.E., J.-O.A., and M.J.C. commented on the manuscript, and A.S.D. revised it. All authors read and approved the final manuscript.

Funding: This research was funded by Svenskt Vattenkraftcentrum, SVC ("The Swedish Hydropower Center").

Acknowledgments: The study was performed as part of Svenskt Vattenkraftcentrum, SVC ("The Swedish Hydropower Center"). SVC was established by the Swedish Energy Agency, Energiforsk and Svenska Kraftnät with Luleå University of Technology, The Royal Institute of Technology, Chalmers University of Technology and Uppsala University (www.svc.nu). Measurements took place in the Porjus Hydropower Center facility—A foundation run by Vattenfall, Andritz Hydro and GE Renewables.

Conflicts of Interest: The authors declare no conflict of interest.

References

1. Trivedi, C.; Gandhi, B.; Michel, C.J. Effect of transients on Francis turbine runner life: A review. *J. Hydraul. Res.* **2013**, *51*, 121–132. [CrossRef]
2. Bakken, B.H.; Bjorkvoll, T. Hydropower unit start-up Costs. In Proceedings of the IEEE Power Engineering Society Summer Meeting, Chicago, IL, USA, 21–25 July 2002.
3. Nilsson, O.; Sjelvgren, D. Hydro unit start-up costs and their impact on the short term scheduling strategies of Swedish power producers. *IEEE Trans. Power Syst.* **1997**, *12*, 38–44. [CrossRef]
4. Goyal, R.; Cervantes, M.J.; Gandhi, B.K. Synchronized PIV and pressure measurements on a model Francis turbine during start-up. *J. Hydraul. Res.* **2019**, *57*, 1–17. [CrossRef]
5. Presas, A.; Luo, Y.; Wang, Z.; Guo, B. Fatigue life estimation of Francis turbines based on experimental strain measurements: Review of the actual data and future trends. *Renew. Sustain. Energy Rev.* **2019**, *102*, 96–110. [CrossRef]
6. Huang, X.; Chamberland-Lauzon, J.; Oram, C.; Klopfer, A.; Ruchonnet, N. Fatigue analyses of the prototype Francis runners based on site measurements and simulations. In Proceedings of the 27th IAHR Symposium on Hydraulic Machinery and Systems (IAHR 2014), Montreal, QC, Canada, 22–26 September 2014.

7. Morissette, J.F.; Chamberland-Lauzon, J.; Nennemann, B.; Monette, C.; Giroux, A.M.; Coutu, A.; Nicolle, J. Stress predictions in a Francis turbine at no-load operating regime. In Proceedings of the 28th IAHR symposium on Hydraulic Machinery and Systems (IAHR2016), Grenoble, France, 4–8 July 2016.
8. Coutu, A.; Gagnon, M.; Monette, C. *Life Assessment of Francis Runners Using Strain Gage Site Measurements*; Waterpower XV: Chattanooga, TN, USA, 2007.
9. Löfflad, J.; Eissner, M. Life time assessment and plant operation optimization based on geometry scan and strain gauge testing–START/STOP optimization. In Proceedings of the 10th International Conference on Hydraulic Efficiency Measurements (IGHEM 2014), Itajuba, Brasil, 16 September 2014.
10. Gagnon, M.; Jobidon, N.; Lawrence, M.; Larouche, D. Optimization of turbine startup: Some experimental results from a propeller runner. In Proceedings of the 27th IAHR Symposium on Hydraulic Machinery and Systems (IAHR 2014), Montreal, QC, Canada, 22–26 September 2014.
11. Gagnon, M.; Tahan, S.A.; Bocher, P.; Thibault, D. Impact of startup scheme on Francis runner life expectancy. In Proceedings of the 25th IAHR Symposium on Hydraulic Machinery and Systems, Timisoara, Romania, 20–24 September 2010.
12. Valentín, D.; Presas, A.; Bossio, M.; Egusquiza, M.; Egusquiza, E.; Valero, C. Feasibility of detecting natural frequencies of hydraulic turbines while in operation, using strain gauges. *Sensors* **2018**, *18*, 174. [CrossRef] [PubMed]
13. Trivedi, C.; Gogstad, P.J.; Dahlhaug, O.G. Investigation of the unsteady pressure pulsations in the prototype Francis turbines during load variation and startup. *J. Renew. Sustain. Energy* **2017**, *9*, 064502. [CrossRef]
14. Jansson, I. Vibrant Bodies of Swirling Flow: On the Limits of Mechanical Power Transformation. Ph.D. Thesis, Luleå University of Technology, Luleå, Sweden, 2013.
15. Trivedi, C.; Cervantes, M.J.; Gandhi, B.K.; Ole, D.G. Experimental investigations of transient pressure variations in a high head model Francis turbine during start-up and shutdown. *J. Hydrodyn* **2014**, *26*, 277–290. [CrossRef]
16. Trivedi, C.; Cervantes, M.J.; Dahlhaug, O.G.; Gandhi, B.K. Experimental investigation of a high head Francis turbine during spin-no-load operation. *J. Fluids Eng.* **2015**, *137*, 061106. [CrossRef]
17. Amiri, K.; Mulu, B.; Raisee, M.; Cervantes, M. Experimental study on flow asymmetry after the draft tube bend of a Kaplan turbine. *Adv. Appl. Fluid Mech.* **2016**, *19*, 441–472.
18. Coulaud, M.; Lemay, J.; Deschenes, C. Analysis of the runner behavior during the start-up sequence in a bulb turbine model. *J. Fluids Eng.* **2019**, *141*, 081106. [CrossRef]
19. Coulaud, M.; Fraser, R.; Lemay, J.; Duquesne, P.; Aeschlimann, V.; Deschênes, C. Preliminary investigation of flow dynamics during the start-up of a bulb turbine model. In Proceedings of the 28th IAHR Symposium on Hydraulic Machinery and Systems (IAHR2016), Grenoble, France, 4–8 July 2016.
20. Nicolle, J.; Morissette, J.F.; Giroux, A.M. Transient CFD simulation of a Francis turbine startup. In Proceedings of the 26th IAHR Symposium on Hydraulic Machinery and Systems, Beijing, China, 19–23 August 2012.
21. Nicolle, J.; Giroux, A.M.; Morissette, J.F. CFD configurations for hydraulic turbine startup. In Proceedings of the 27th IAHR Symposium on Hydraulic Machinery and Systems (IAHR 2014), Montreal, QC, Canada, 22–26 September 2014.
22. Morissette, J.F.; Nicolle, J. Fluid-structure simulations of the stochastic behaviour of a medium head Francis turbine during startup. In Proceedings of the 29th IAHR Symposium on Hydraulic Machinery and Systems, Kyoto, Japan, 16–21 September 2018.
23. Li, Z.; Bi, H.; Wang, Z.; Yao, Z. Three-dimensional simulation of unsteady flows in a pump-turbine during start-up transient up to speed no-load condition in generating mode. *Proc. Inst. Mech. Eng. A J. Power Energy* **2016**, *230*, 570–585. [CrossRef]
24. Minakov, A.; Sentyabov, A.; Platonov, D. *Numerical Investigation of Flow Structure and Pressure Pulsation in the Francis-99 Turbine during Startup*; Francis-99 Workshop 2: Transient Operation of Francis Turbines; IOP Publishing: Bristol, UK, 2017.
25. Staubli, T.; Senn, F.; Sallaberger, M. *Instability of Pump-Turbines during Start-Up in Turbine Mode*; Hydro 2008: Ljubljana, Slovenia, 2008.
26. Melot, M.; Coulaud, M.; Chamberland-Lauzon, J.; Nennemann, B.; Deschênes, C. Hydraulic turbine start-up: A fluid-structure simulation methodology. In Proceedings of the 29th IAHR Symposium on Hydraulic Machinery and Systems, Kyoto, Japan, 17–21 September 2018.

27. He, L.Y.; Wang, Z.W.; Kurosawa, S.; Nakahara, Y. Resonance investigation of pump-turbine during startup process. In Proceedings of the 27th IAHR Symposium on Hydraulic Machinery and Systems (IAHR 2014), Montreal, QC, Canada, 22–26 September 2014.
28. Cervantes, J.M.; Soltani Dehkharqani, A. Prototype Kaplan turbine measurements: Instrumentation overview. In Proceedings of the 2nd IAHR-Asia Symposium on Hydraulic Machinery and Systems, Busan, Korea, 24–25 September 2019.
29. Press, W.H.; Teukolsky, S.A. Savitzky-Golay smoothing filters. *Comput. Phys.* **1990**, *4*, 669–672. [CrossRef]
30. Houde, S.; Dumas, G.; Deschênes, C. Experimental and numerical investigations on the origins of rotating stall in a propeller turbine runner operating in no-load conditions. *J. Fluids Eng.* **2018**, *140*, 111104. [CrossRef]
31. Půlpitel, L.; Skotak, A.; Koutnik, J. *Vortices Rotating in the Vaneless Space of a Kaplan Turbine Operating under Off-Cam High Swirl Flow Conditionsspringer*; Kluwer Academic: London, UK, 1996; pp. 925–934.